Critical Care

RESEARCH

Open Access

Development and validation of intracranial hypertension prediction models based on radiomic features in patients with traumatic brain injury: an exploratory study based on CENTER-TBI data

Yingchi Shan[1], Yajun Xue[1], Jun Zhu[4], Thijs Vande Vyvere[5,6], Dana Pisică[7,8], Andrew Maas[9,10], Shuo Zhang[2,3†] and Guoyi Gao[2,3*†]

Abstract

Background Head computed tomography (CT) is a routinely performed examination to assess the intracranial condition of patients with traumatic brain injury (TBI), and radiological findings can help to indicate the presence of intracranial hypertension. At present, the prediction of intracranial hypertension is mainly based on manual discrimination of imaging characteristics. The aim of our study was to establish a model to predict intracranial hypertension via fully automatic CT image segmentation, rigorous radiomic feature extraction and reliable model development and validation.

Methods Patients admitted to the intensive care unit (ICU) who underwent intracranial pressure (ICP) monitoring were included in our study. For the development cohort, we extracted data from the CENTER-TBI database and randomly divided the data into a training group and a test group. For the validation cohort, we extracted data from patients admitted to the Shanghai General Hospital. Patients whose initial recorded ICP value was greater than or equal to 20 mmHg were defined as having intracranial hypertension. Radiological features, including imaging characteristics and three categories of radiomic features, were extracted from the head CT. Feature selection was performed for all radiological findings. A morphological model was built on the basis of selected imaging characteristics. First-order, second-order and third-order models were built on the basis of selected radiomic features. A comprehensive model was built on the basis of all selected radiological findings. The performances of these five models were assessed by four classifiers, including logistic regression (LR), random forest (RF), multilayer perceptron (MLP), and extreme gradient boosting (XGB), from which the best classifier was selected. After the process of model training and external validation, we ultimately used the optimal classifier to generate a prediction model with greater predictive power and stability.

†Shuo Zhang and Guoyi Gao have contributed equally to this work.

First authors: Yingchi Shan and Yajun Xue

*Correspondence:
Guoyi Gao
gao3@sina.com
Full list of author information is available at the end of the article

Results Five models were built, including a morphological model, first-order model, second-order model, third-order model and comprehensive model. The optimal classifier was the logistic regression (LR) classifier, with which the morphological, first-order, second-order, third-order and comprehensive models had AUCs of 0.75, 0.77, 0.76, 0.86, and 0.83 and F1 scores of 0.54, 0.73, 0.63, 0.72, and 0.75, respectively, in the external validation group.

Conclusions We successfully established a model for predicting intracranial hypertension on the basis of radiomic features. This model may serve as an approach for intracranial hypertension prediction in TBI patients.

Keywords Traumatic brain injury, Radiomic features, Intracranial hypertension, Prediction

Introduction

Traumatic brain injury is a critical condition in neurosurgery, with high rates of disability and mortality [1]. Previous studies have consistently shown that early posttraumatic intracranial hypertension in TBI patients often indicates poor outcomes [2, 3]. Therefore, actively seeking effective indicators for assessing ICP is crucial. Head computed tomography (CT) is an imaging technique that can provide rapid results and is highly sensitive to hemorrhages. Thus, this technique is widely used for early TBI diagnosis and constitutes an essential means of assessing patient conditions, providing a basis for predicting the development of intracranial hypertension [4, 5]. More importantly, repeat CT scanning is the main component of the Consensus Revised Imaging and Clinical Examination (CREVICE) protocol, which is advocated for settings in which more advanced neuromonitoring (including ICP monitoring) is not available. In interpreting head CT scans, the transition from the use of subjective clinical experience to the analysis of objective radiomic data plays a critical role [6]. The former identifies typical imaging characteristics on the basis of overall morphological changes in the images, whereas the latter provides detailed features on the basis of texture deconstruction in the images [7]. ICP prediction using head CT scans is primarily dependent on a fully supervised model based on clinical experience [8]. This approach is a semantic analysis mode based on grayscale thresholds and morphological changes. While radiomic features have been incorporated in some studies, these studies have focused on changes in pixel grayscale values, which are the first-order radiomic features, without the analysis of pixel spatial distribution based on grayscale values, which are the second-order and third-order radiomic features [9, 10]. The aim of our study was to explore fully automated CT image segmentation to improve model prediction ability through categories of radiomic features. Ultimately, the goal of this study was to establish an intracranial hypertension prediction model based on CT image analysis with clinical credibility.

Methods

Research patients

The development population was drawn from the prospective observational study of Collaborative European Neurotrauma Effectiveness Research in TBI (CENTER-TBI), registered at clinicaltrials.gov (NCT02210221). We included TBI patients admitted to the ICU who underwent ICP monitoring. The validation cohort consisted of TBI patients from Shanghai General Hospital admitted between 2022 and 2023. The study protocol and consent forms were approved by the Ethics Committee of Shanghai General Hospital (NO: CTCCR-2021B10). The specific criteria were as follows.

Inclusion criteria: (1) patients aged between 18 and 65 years; (2) patients who underwent ICP probe implantation (the location of the probe was inside the brain parenchyma or the ventricle) without craniotomy; (3) patients whose ICP records and head CT images were collected and stored electronically; and (4) patients whose hematomas or contusions shown on CT were all located supratentorially.

Exclusion criteria: (1) patients with a prior history of TBI, intracranial tumors, or cerebral vascular diseases that may lead to changes in cranial cavity structures; and (2) patients with missing or unclear information in CT images or ICP metrics.

Patients screened and included in the CENTER-TBI database were randomly divided into training and test groups at a 4:1 ratio. TBI patients from Shanghai General Hospital were included for external validation of the model. Furthermore, to avoid the scenario where the quantity of collected samples failed to satisfy the lower limit for model validation, we calculated the minimum number of samples to be collected through relatively straightforward predictive methods. On the basis of the statistics that the percentage of patients with intracranial hypertension among the enrolled patients in this study was 21%, the significance level alpha was set to 0.05, and the statistical power was set to 0.8, leading to a required sample size for the external validation group of at least 74 patients under the hypothesis that the difference in the percentage of patients with intracranial hypertension between the estimated external validation dataset and the

previous dataset is within 21%. The estimated value was calculated by the 'zt_ind_solve_power' function in the 'statsmodels' module in Python 3.7.13.

Data collection

The following patient information was collected from the CENTER-TBI database as well as the Shanghai General Hospital medical records database for patients in the validation group.

(1) Baseline information: sex, age, preoperative Glasgow Coma Scale (GCS) score, preoperative pupillary reflex, blood pressure, and whether surgery was needed.
(2) The initial recorded ICP value obtained closest to the time the preoperative CT scan was obtained and the time interval between them.
(3) CT images: the last preoperative CT images of the patients in Nifti format and the imaging characteristics and the radiomic features obtained from CT images.

Image processing

(1) *Acquisition of imaging characteristics*: A total of 15 imaging characteristics were scored by senior neurosurgeons upon review of the CT images: midline shift greater than 5 mm, cisternal compression (quadrigeminal cistern/cisterna magna/ambient cistern/suprasellar cistern), cerebral herniation (left subfalcine herniation/right subfalcine herniation/left transtentorial herniation/right transtentorial herniation/tonsillar herniation), cortical sulcus effacement, ventricular compression (fourth ventricle/third ventricle), mass lesion, and cerebral edema. The midline shift was determined by measuring the width of the cranial cavity and the distance from the lateral skull to the foramen of Monro at the level of the foramen of Monro. The status of the basal cisterns, ventricular compression and brain herniation characteristics were assessed on slices of the corresponding anatomical structures. All the imaging findings are shown in Fig. 1 (the imaging findings are shown from the sequence 'a' to 'o' in the figure). a: midline shift greater than 5 mm; b: quadrigeminal cistern compression; c: cisterna magna compression; d: ambient cistern compression; e: suprasellar

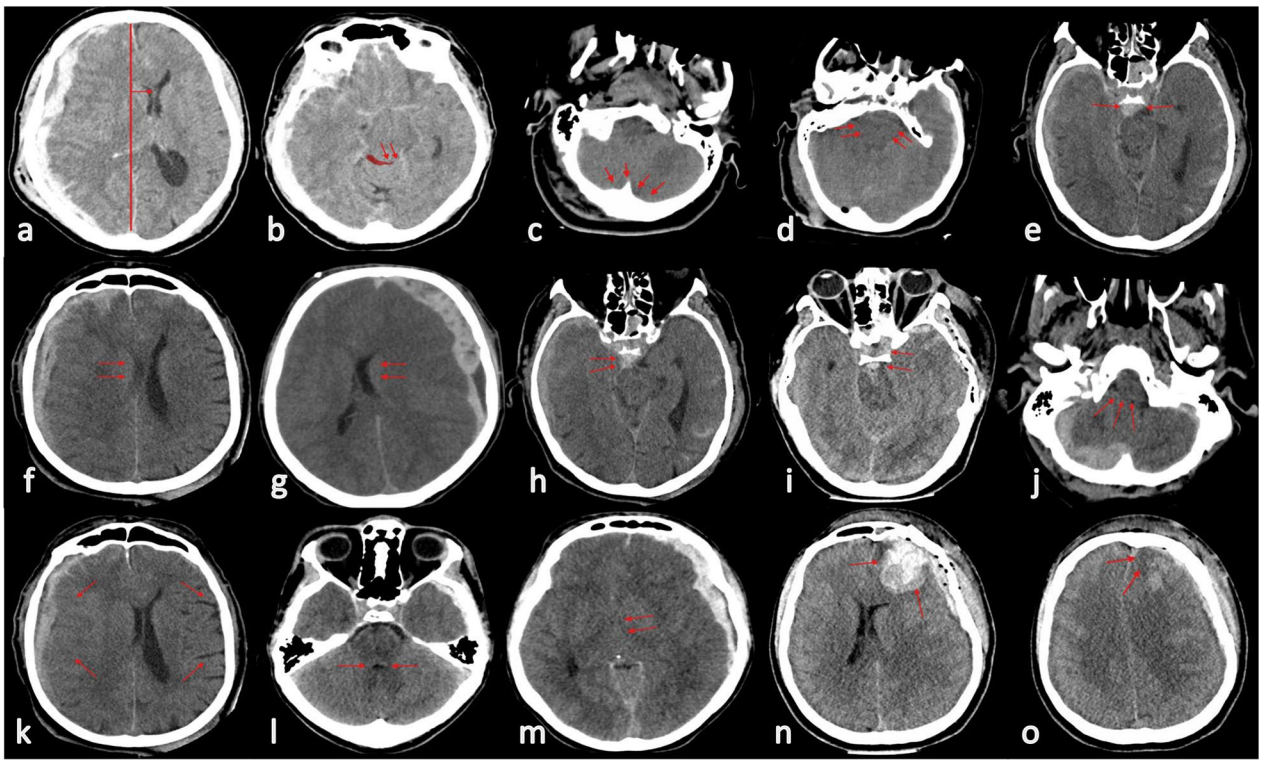

Fig. 1 Measurements of 15 imaging findings

cistern compression; f: left subfalcine herniation; g: right subfalcine herniation; h: left transtentorial herniation; i: right transtentorial herniation; j: tonsillar herniation; k: cortical sulcus effacement; l: fourth ventricle compression; m: third ventricle compression; n: mass lesion; o: cerebral edema).

(2) *Acquisition of radiomic features*: We adopted a fully automatic method for selecting target slices and segmenting the region of interest (ROI) in CT images. In this study, target slices were defined as all slices containing hematomas, and the ROI was defined as the brain region after removing the skull structure on the target slices. All the processes were performed in Python 3.7.13. The detailed algorithm of ROI segmentation and target slice selection is shown in Appendix V.

ROI segmentation

The aim of ROI segmentation was to select the optimal contour from the CT images on each layer. In this study, parts with significant grayscale changes were defined as edges, and the areas surrounded by edges were defined as contours. Therefore, any closed shape could constitute a contour in a CT image. After excluding mixed signal interference outside the head structure, the original CT image containing the skull had the largest contour. The desired optimal contour to be found was the largest contour after removing the skull. Because patients with traumatic brain injury often have skull defects caused by fractures, in this study, we applied the concept of a convex hull to avoid concave situations. To find the optimal contour, additional prior constraints on the image were applied as follows:

(a) On the basis of a gray value of 127, the image was first binarized and then eroded/dilated to eliminate white noise, the image was smoothed, and then the edges and contours were found.
(b) The largest contour satisfying the condition based on the convex hull (any line connecting two points inside the shape remains within the contour) was extracted, and it was ensured that there were no bright points exceeding the 97th percentile within the contour.
(c) The above steps were repeated to perform a secondary extraction on the contour (aiming to eliminate interference signals within the contour caused by the convex hull).
(d) The extracted contour was shrunk inward by 10 pixels to minimize the impact of bright points in the surrounding area.

Target slice selection

After all slices with prior constraints were processed, the slices containing hematomas needed to be selected to segment the region of interest (ROI). In this study, the hematoma area in the CT scan was defined as bright spots (the CT value range was set to 50–100 Hounsfield units). All the bright spots constituted the hematoma area, and a chain of continuous bright spots contained the target slices to be extracted. The specific steps were as follows:

(e) The area of all layers was calculated, and if the current area was less than 0.9 times the maximum area and subsequent layers met the condition, then the current and subsequent layers were deleted.
(f) Layers that satisfied step one were searched for all bright spot contours, the bright spots were expanded by 5 pixels outward, and if there was an intersection with a bright spot from the previous layer, it was recorded in the bright spot chain; otherwise, it was recorded as the starting point of the bright spot chain.
(g) All layers were iterated through, recording all bright spots and bright spot chains (condition: more than three bright spots).

After the ROI segmentation was completed, we resampled all the ROIs (voxel normalization): the simple TK module was used to read the spacing and size of the original image, a uniform new spacing was set as (1, 1, 1), and the corresponding new size was obtained. Then, the radiomic features, including first-order, second-order, and third-order features, were extracted via the 'PyRadiomics' module in Python 3.7.13, with values of 32, 40, and 35, respectively. First-order features focused mainly on basic image intensity information, reflecting the fundamental grayscale characteristics of the lesion. Second-order features concentrated on the relationships between pixel pairs, which can reveal the subtle internal structure of the lesion. Third-order features, from a more complex spatial distribution perspective, presented the overall characteristics of the lesion. The definition of each feature is listed in the supplemental file (Appendix II). The entire radiomic feature extraction process is shown in Fig. 2.

Data processing

Patients were grouped on the basis of the initial recorded ICP. Patients whose initial recorded ICP value was greater than or equal to 20 mmHg were defined as having intracranial hypertension. Univariate analysis was used to examine the distribution of characteristics between patients with an ICP $\geq$ 20 mmHg and those with

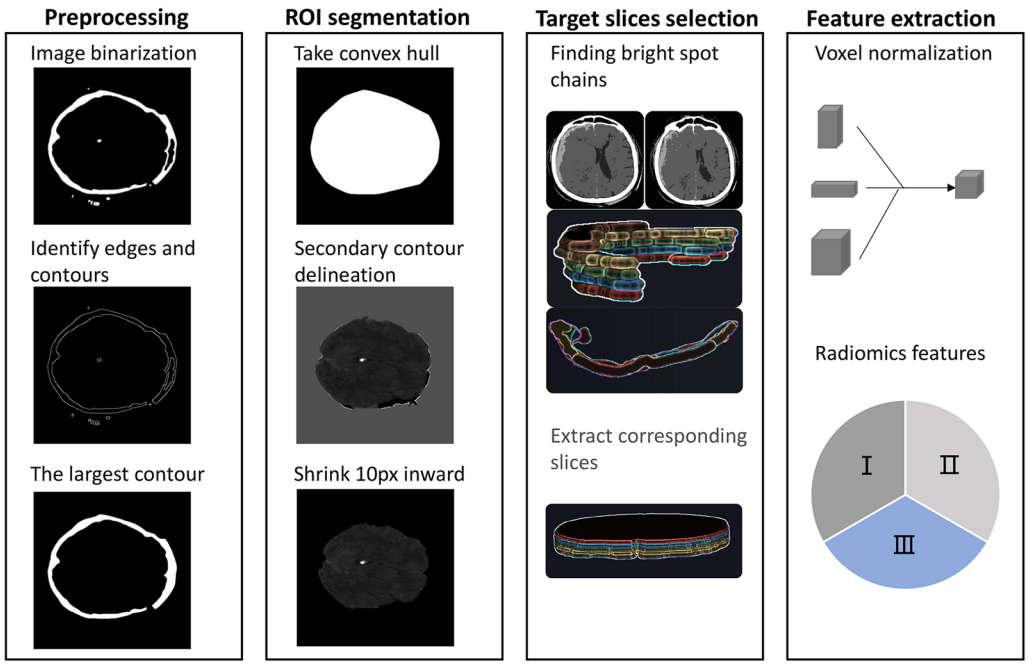

Fig. 2 Radiomics features extraction process

an ICP < 20 mmHg. The data were then divided into a training set and a test set at a ratio of 8:2. The imputation was carried out for the baseline parameters that were found to be missing during the data collection process. Specifically, we used the random forest algorithm to impute the remaining data with missing values (presented as null values or blank values) [11]. Considering the unbalanced data of the negative and positive groups, the positive data of the training set were augmented by the smote oversampling method [12]. For 15 categorical variables representing imaging characteristics, Spearman correlation analysis was used to describe their interdependency, and then the appropriate imaging characteristics were selected for further analysis. For radiomic features, we utilized recursive feature elimination (RFE) to calculate feature importance and determine the optimal number of features on the basis of feature importance to reduce the feature dimension from the primary extracted features.

Model establishment

During the preliminary phase, we carried out a correlation analysis of the imaging characteristics and computed the feature importance of the radiomic features. Subsequently, we carefully selected those features that could most effectively capture the characteristics of the image and significantly increase the accuracy and stability of the model. On the basis of these selected imaging characteristics and radiomic features, we constructed five models for predicting whether a patient has intracranial hypertension, namely, the morphology model, first-order model, second-order model, third-order model, and comprehensive model. The morphological model encompassed imaging characteristics, whereas the other three models encompassed three categories of radiomic features. The comprehensive model encompassed selected imaging characteristics and radiomic features. Before processing the data with different classifiers, we adopted min–max normalization, which was completed in advance so that it would not cause errors due to different evaluation contents among various classifiers. For each model, we performed a fivefold cross-validation on the training groups, whereas the cases from the testing groups were used for model evaluation. The performance of the model was evaluated by four classifiers, including logistic regression (LR), random forest (RF), multilayer perceptron (MLP), and extreme gradient boosting (XGB). The best-performing classifier was selected to establish the final presented intracranial hypertension prediction model. The generalization performance of the model was evaluated using patient data from the external validation cohort. The model performance was visualized by plotting the receiver operating characteristic (ROC) curve and by calculating the area under the curve (AUC), accuracy, precision, recall, and F1 score. The workflow, which includes data collection, image processing, and model establishment, is shown in Fig. 3. Additionally, the

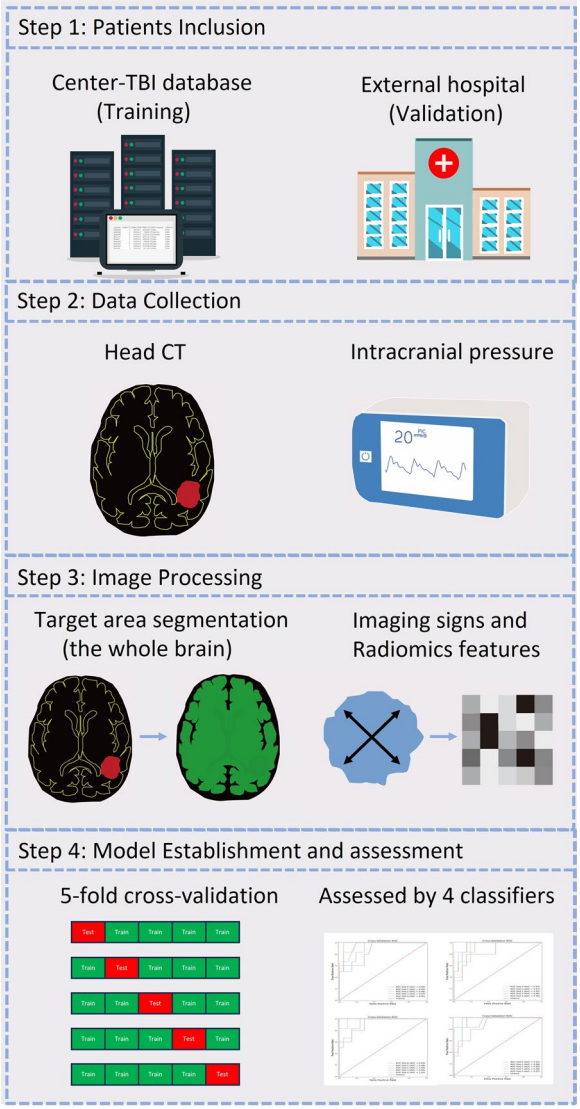

Fig. 3 Workflow of the study

complete code for model training is included in the supplemental file (Appendix VI).

Statistical approach

The patients' baseline data were analyzed via Python 3.7.13 from the Python Software Foundation. Mean values with standard deviations were used to describe continuous variables, whereas frequencies and percentages were used to describe categorical variables. The Kolmogorov–Smirnov (KS) test was used to determine if the continuous variables followed a normal or non-normal distribution. The Levene test was employed to test the homogeneity of continuous variance. Differences between groups were compared using either the Mann–Whitney U test or Student's t test, whereas the chi–square test or Fisher's exact test was used to compare differences. A statistically significant result was considered if the two-sided p value was less than 0.05.

Table 1 The baseline information of three groups

Model	Accuracy	Precision	Recall	FI Score	AUC
Morphology model	0.63	0.74	0.61	0.54	0.75
First-order model	0.82	0.69	0.67	0.73	0.77
Second-order model	0.72	0.62	0.58	0.63	0.76
Third-order model	0.79	0.64	0.71	0.72	0.86
Comprehensive model	0.81	0.72	0.63	0.75	0.83

Results

Baseline characteristics of patients

A total of 4509 patients with head CT data from CENTER-TBI were screened. Among them, 911 patients had ICP records. After patients who did not meet the requirements for CT images and those with missing medical information were excluded, a total of 882 individuals were included in the study. Among them, 705 were included in the training group, while the remaining 177 were included in the testing group. Eighty-four patients from Shanghai General Hospital were included in the external validation group. The baseline characteristics of the three groups are shown in Table 1. Among the patients who underwent subsequent surgeries, 520 patients in the CENTER-TBI dataset underwent simple craniotomy for hematoma evacuation, 63 patients underwent left decompressive craniectomy, 85 patients underwent right decompressive craniectomy, and 21 patients underwent bilateral decompressive craniectomy. In the external validation dataset, 30 patients underwent simple craniotomy for hematoma evacuation, 18 patients underwent left decompressive craniectomy, 15 patients underwent right decompressive craniectomy, and 4 patients underwent bilateral decompressive craniectomy. The mean and standard deviation of the time interval between the ICP measurement and the CT examination in the training, testing, and external validation group were 2.83 ± 0.94 h, 2.37 ± 1.40 h, and 2.57 ± 1.36 h, respectively.

Multicollinearity analysis and feature selection

Collinearity analysis revealed that the three variables "midline shift greater than 5 mm", "right subfalcine herniation", and "left subfalcine herniation" had variance inflation factors (VIFs) greater than 10, specifically, 62.884, 48.918, and 28.673, respectively. Hence, these features were excluded, and the remaining 12 imaging features were retained to construct the morphological

model. The specific correlation coefficient heatmap can be found in Appendix I. After recursive feature elimination, 18 first-order features, 20 s-order features and 14 third-order features were selected. The detailed radiomic features selected through RFE and the primary features can be found in Appendix II.

Establishment and performance of the models

Univariate analysis revealed no significant difference between patients with intracranial hypertension and patients without intracranial hypertension in the training, testing and validation groups ($p > 0.05$). We finally established the morphology model, first-order model, second-order model, third-order model and comprehensive model, which had AUCs of 0.75, 0.77, 0.76, 0.86, and 0.83 and F1 scores of 0.54, 0.73, 0.63, 0.72, and 0.75, respectively, in the external validation group. The ROC curve after fivefold cross-validation on the training groups and testing groups can be found in Appendix III. The ROC curves for the four models with single radiological findings in the validation group are shown in Fig. 4, and the LR classifier performed best in each model. The ROC curve of the comprehensive model using the LR classifier is shown in Fig. 4. The accuracy, precision, recall, F1 score and AUC of all the models when the LR classifier was used are shown in Table 2. The results of the other classifiers can be found in Appendix IV.

Discussion

In this study, we analyzed CT images of patients with TBI from the CENTER-TBI database and extracted imaging characteristics and radiomic features to predict intracranial hypertension. Radiomic features had a strong ability to predict intracranial hypertension, surpassing morphological imaging characteristics. When combining radiomic features and imaging characteristics, the model maintained high predictive ability and was more stable (with a higher F1 score).

Timely and accurate evaluation of intracranial hypertension is vital for making effective decisions in TBI management. Invasive parenchymal or intraventricular ICP probes are standard procedures for monitoring intracranial pressure. No robust noninvasive approaches exist to monitor IVP continuously, although transcranial Doppler monitoring and optic nerve sheath diameter measurement offer potential, and efforts in analyzing radiological images such as CT and MR images are continuing [13, 14].

In recent years, various studies have highlighted the value and potential of radiomics in diagnosing and treating neurological disorders, as it is recognized in academia for its robustness and adaptability [15, 16]. Radiomics is also commonly used to analyze spatial relationships between pixel values in images and can quantitatively describe "invisible" image changes [17]. Bo and colleagues constructed a combined model of radiomic features and clinical features to predict hematoma enlargement and

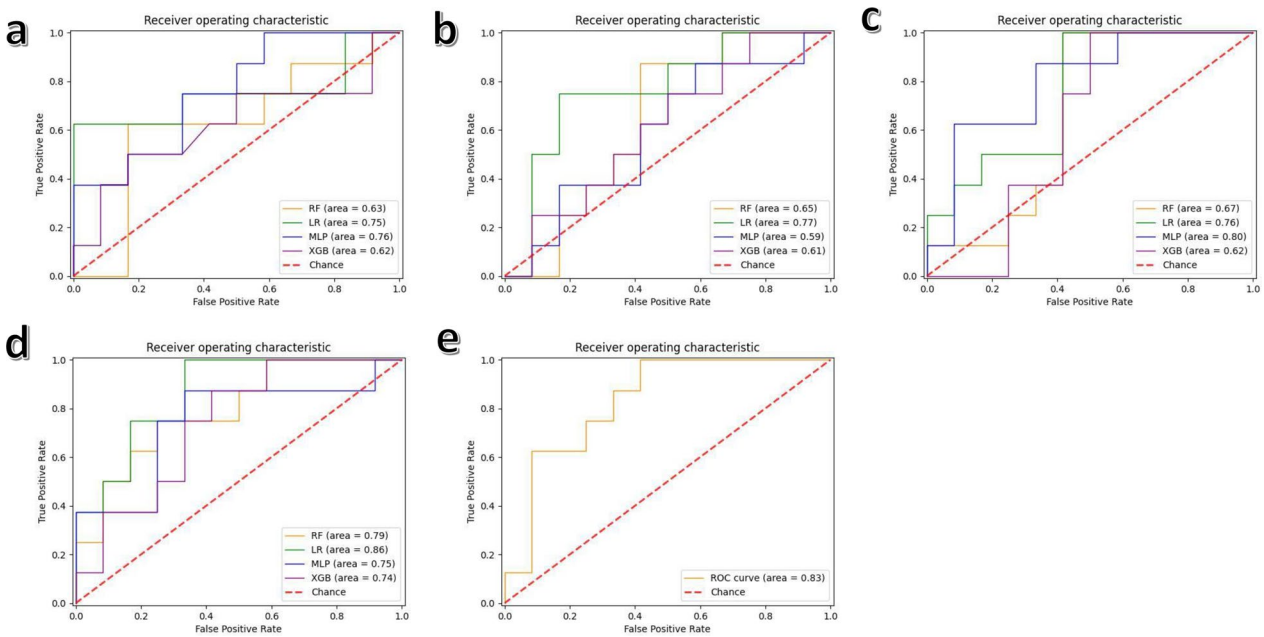

Fig. 4 ROC of four separate models and the comprehensive model. **a**: morphology model; **b**: first-order model; **c**: second-order model; **d**: third-order model; **e**: the comprehensive model

Table 2 Accuracy, precision, recall, FI score and AUC of all models using LR classifier in external validation dataset

Characteristics	Training group (N = 705)	Testing group (N = 177)	Validation group (N = 84)
Sex			
Male (%)	492(68.18)	130(90.91)	63(75.82)
Female (%)	213(31.82)	47(9.09)	21(24.18)
Age (mean ± std, years old)	46.26 ± 12.66	44.64 + 12.15	47.75 ± 13.45
GCS (median [IQR])	6[4, 7]	6[4, 7]	6[5, 7]
Pupillary reflex			
Both present (%)	359(52.29)	89(45.46)	40(48.34)
One absent (%)	138(20.92)	46(27.27)	16(19.21)
Both absent (%)	208(26.80)	42(27.27)	28(32.45)
Operation			
Yes (%)	542(76.62)	147(81.82)	67(80.39)
No (%)	158(23.38)	30(18.18)	17(19.61)
Systolic BP (median [IQR], mmHg)	125(116,138]	130(116,130]	130(119,138]
Intracranial hypertension			
Yes (%)	142(20.14)	43(24.29)	20(23.81)
No (%)	563(79.86)	134(75.71)	64(76.19)

clinical prognosis and reported promising results [18]. Nomograms based on radiomic features have been developed in multiple studies and have shown significant value in predicting mortality and clinical outcomes after TBI [19, 20]. Therefore, combining multiple features, primarily radiomic features, appears to be a promising approach for informing clinical prediction. The reason may be that radiomics effectively compensates for "subjective errors" or confounders, which may be present when imaging characteristics are assessed. For example, midline shift in patients with bilateral cranial injuries may not always be evident [21], and diffuse axonal injury patients often lack typical characteristics on CT scans [22]. Therefore, what is not visible is not necessarily absent and can be detected by radiomics, thus providing more detailed information. However, relatively few studies on the prediction of adverse events such as intracranial hypertension using radiomics exist. In our study, we analyzed radiomic features, and we confirmed their powerful ability to predict intracranial hypertension. Combining radiomic features with imaging characteristics increased the dimensionality of the model, thereby increasing the resolution of the model predictions (the F1 score of the comprehensive model increased).

In constructing and evaluating a single model, with the exception of the morphological model that incorporates 12 features, the other three models include 18, 20 and 14 features, respectively. The current sample size determines this to ensure the statistical power of the study. The best single model was constructed with third-order features (AUC = 0.86), suggesting that it may be the preferred prediction indicator for imaging analysis in TBI patients, especially considering computational costs and convenience. Compared with a single model, a comprehensive model can capture more information about textures related to CT images, improving predictive performance. Possible reasons for the improved prediction performance of the comprehensive model include the following: (1) the features provide essentially complementary information to comprehensively characterize the ICP from multiple angles, such as gray, morphological, and spatial angles; (2) different features are relatively independent, and collinearity analysis of imaging characteristics is also carried out to ensure low correlation between different features.

We developed a protocol for a fully automated ROI segmentation algorithm based on grayscale thresholds and morphological structures. The aim of the protocol was to minimize the radiomic limitation of poor reproduction. In addition, for the segmentation of the ROI in this study, the segmented area is defined as all intracranial areas after the skull is removed. It is generally believed that delineating the ROI should follow the contour of the lesions layer by layer, and the ideal segmentation standard for the ROI does not include any normal tissues, which is the main idea behind current ROI segmentation. We included regions in the ROI area that contained both lesion tissue and normal tissue, contrary to the traditional approach of ROI extraction [23, 24]. The reason for this difference lies in the fact that the primary goal of traditional radiomic analysis is to reveal the nature of lesion areas,

whereas the predicted indicator in this study was the ICP, a parameter reflecting the overall intracranial condition. Therefore, the choice of ROI in this study included the overall brain structures (including hematomas, edema, and ventricles).

Limitations of this study include the following aspects: (1) During the patient inclusion process, patients with elevated ICP in whom ICP monitors were not placed were not identified as high-risk patients and were thus excluded. (2) There was a time interval between the head CT examination and the ICP measurement. Additionally, in the present study, we did not record the time intervals from the occurrence of the event to the CT examination or from admission to the CT examination. (3) In the process of image segmentation, we analyzed the brain region on slices containing hematomas, not the whole-brain region. Therefore, we were unable to obtain a complete understanding of the voxel changes caused by TBI in the entire three-dimensional space of the skull cavity. Additionally, algorithms that focus on slices with hematomas, while accurately extracting radiomic features related to hematomas, may miss crucial markers of intracranial hypertension, such as edema or tonsillar herniation. (4) When a model is constructed, manual labeling of morphological features is indeed indispensable because the accuracy of data labeling can be ensured. However, there are also drawbacks to the use of this method, as it is labor intensive and affected by subjective factors. (5) In this study, the traditional semantic method was used in image segmentation, which results in a certain degree of information loss. In subsequent research, a deep learning model can be used to better exploit the abundance of image information.

Conclusion

In this study, we successfully constructed intracranial hypertension prediction models on the basis of data from the CENTER-TBI database via radiomic and imaging characteristics. These models were externally validated on an independent cohort from China. A fully automated CT image segmentation method was adopted to improve the objectivity of the models. Models based on radiomic features performed well in both the development and validation cohorts. Combining radiomic features with imaging characteristics improved model performance, providing a novel and promising method for the prediction of intracranial hypertension using CT image analysis.

Availability of supporting data

We do not have any research data outside the submitted manuscript file.

Abbreviations

AUC	Area under the curve
CENTER-TBI	Collaborative European Neurotrauma Effectiveness Research in TBI
CREVICE	Consensus revised imaging and clinical examination
CT	Computed tomography
ICP	Intracranial pressure
ICU	Intensive care unit
KS	Kolmogorov–Smirnov
LR	Logistic regression
MLP	Multilayer perceptron
RF	Random forest
RFE	Recursive feature elimination
ROI	Region of interest
TBI	Traumatic brain injury
VIF	Variance inflation factors
XGB	Extreme gradient boosting

Supplementary Information

The online version contains supplementary material available at https://doi.org/10.1186/s13054-025-05328-4.

Additional file1 (DOCX 1415 KB)

Acknowledgements

We would like to express our sincere gratitude. This study was supported by the Beijing Natural Science Foundation (grant number: J230008) and the National Key R&D Program of China (grant number: 2023YFC2410605). Their support has been instrumental in enabling the successful completion of this research.

Author contributions

Study concept and design: Y.S., S.Z., G.G.. Acquisition, analysis or interpretation of data: Y.X., J.Z.. First drafting of manuscript: Y.S., Y.X., S.Z., G.G.. Critical revision for important intellectual content and final approval of manuscript: Y.S., Y.X., J.Z., T.V.V., D.P., A.M.,S.Z.,G.G.. All authors reviewed the manuscript.

Funding

This work was supported by Beijing Natural Science Foundation (grant number: J230008); the National Key R&D Program of China (grant number: 2023YFC2410605); the National Natural Science Foundation of China (grant number: 82401612) and the funding from Beijing Neurosurgical Institute.

Declarations

Ethical approval and consent to participate

The development population was drawn from the prospective observational study of Collaborative European Neurotrauma Effectiveness Research in TBI (CENTER-TBI), registered at clinicaltrials.gov (NCT02210221). The study protocol and consent forms were approved by the Ethics Committee of Shanghai General Hospital (NO: CTCCR-2021B10).

Consent for publication

The results/data/figures in this manuscript have not been published elsewhere, nor are they under consideration (from you or one of your contributing authors) by another publisher.

Competing interests

We declare that the authors have no competing interests as defined by BMC or other interests that might be perceived to influence the results and/or discussion reported in this paper.
The authors declare no competing interests.

Author details

[1]Department of Neurosurgery, School of Medicine, Shanghai General Hospital, Shanghai Jiao Tong University, Shanghai, China. [2]Department of Neurosurgery, Beijing Tiantan Hospital, Capital Medical University, Beijing, China. [3]Key Laboratory of Central Nervous System Injury, Beijing

Neurosurgical Institute, Capital Medical University, Beijing, China. [4]Department of Neurosurgery, Zhongda Hospital, Southeast University, Nanjing, China. [5]Department of Radiology, Antwerp University Hospital, Antwerp, Belgium. [6]Department of Molecular Imaging and Radiology (MIRA), Faculty of Medicine and Health Science, University of Antwerp, Antwerp, Belgium. [7]Department of Neurosurgery, Erasmus MC—University Medical Center Rotterdam, Rotterdam, The Netherlands. [8]Department of Public Health, Erasmus MC—University Medical Center Rotterdam, Rotterdam, The Netherlands. [9]Department of Neurosurgery, Antwerp University Hospital, Edegem, Belgium. [10]University of Antwerp, Edegem, Belgium.

Received: 6 December 2024 Accepted: 21 February 2025
Published online: 06 March 2025

References

1. Khellaf A, Khan DZ, Helmy A. Recent advances in traumatic brain injury. J Neurol. 2019;266(11):2878–89.
2. Escamilla-Ocanas CE, Albores-Ibarra N. Current status and outlook for the management of intracranial hypertension after traumatic brain injury: decompressive craniectomy, therapeutic hypothermia, and barbiturates. Neurologia (Engl Ed). 2023;38(5):357–63.
3. Harder TJ, Leary OP, Yang Z, Lucke-Wold B, Liu DD, Still MEH, Zhang M, Yeatts SD, Allen JW, Wright DW, et al. Early signs of elevated intracranial pressure on computed tomography correlate with measured intracranial pressure in the intensive care unit and six-month outcome after moderate to severe traumatic brain injury. J Neurotrauma. 2023;40(15–16):1603–13.
4. Sato R, Akiyama Y, Mikami T, Yamaoka A, Kamada C, Sakashita K, Takahashi Y, Kimura Y, Komatsu K, Mikuni N. Deep learning from head CT scans to predict elevated intracranial pressure. J Neuroimaging. 2024;34(6):742–9.
5. Williamson C, Morgan L, Klein JP. Imaging in neurocritical care practice. Semin Respir Crit Care Med. 2017;38(6):840–52.
6. Bijari S, Sayfollahi S, Mardokh-Rouhani S, Bijari S, Moradian S, Zahiri Z, Rezaeijo SM. Radiomics and deep features: robust classification of brain hemorrhages and reproducibility analysis using a 3D autoencoder neural network. Bioengineering. 2024;11(7):643.
7. Zaman S, Dierksen F, Knapp A, Haider SP, Abou Karam G, Qureshi AI, Falcone GJ, Sheth KN, Payabvash S. Radiomic features of acute cerebral hemorrhage on non-contrast CT associated with patient survival. Diagnostics. 2024;14(9):944.
8. Alali AS, Temkin N, Barber J, Pridgeon J, Chaddock K, Dikmen S, Hendrickson P, Videtta W, Lujan S, Petroni G, et al. A clinical decision rule to predict intracranial hypertension in severe traumatic brain injury. J Neurosurg. 2019;131(2):612–9.
9. Kim H, Kim GD, Yoon BC, Kim K, Kim BJ, Choi YH, Czosnyka M, Oh BM, Kim DJ. Quantitative analysis of computed tomography images and early detection of cerebral edema for pediatric traumatic brain injury patients: retrospective study. BMC Med. 2014;12:186.
10. Wu B, Zhang J, Chen J, Sun X, Tan D. Establishment of a model to predict mortality after decompression craniotomy for traumatic brain injury. Brain Behav. 2024;14(4):e3492.
11. Pelgrims I, Devleesschauwer B, Vandevijvere S, De Clercq EM, Vansteelandt S, Gorasso V, Van der Heyden J. Using random-forest multiple imputation to address bias of self-reported anthropometric measures, hypertension and hypercholesterolemia in the Belgian health interview survey. BMC Med Res Methodol. 2023;23(1):69.
12. Dablain D, Krawczyk B, Chawla NV. DeepSMOTE: fusing deep learning and SMOTE for imbalanced data. IEEE Trans Neural Netw Learn Syst. 2023;34(9):6390–404.
13. Kerscher SR, Schoni D, Neunhoeffer F, Wolff M, Haas-Lude K, Bevot A, Schuhmann MU. The relation of optic nerve sheath diameter (ONSD) and intracranial pressure (ICP) in pediatric neurosurgery practice - Part II: influence of wakefulness, method of ICP measurement, intra-individual ONSD-ICP correlation and changes after therapy. Childs Nerv Syst. 2020;36(1):107–15.
14. Zhang X, Medow JE, Iskandar BJ, Wang F, Shokoueinejad M, Koueik J, Webster JG. Invasive and noninvasive means of measuring intracranial pressure: a review. Physiol Meas. 2017;38(8):R143–82.
15. Li G, Li L, Li Y, Qian Z, Wu F, He Y, Jiang H, Li R, Wang D, Zhai Y, et al. An MRI radiomics approach to predict survival and tumour-infiltrating macrophages in gliomas. Brain. 2022;145(3):1151–61.
16. Ziegelmayer S, Reischl S, Harder F, Makowski M, Braren R, Gawlitza J. Feature robustness and diagnostic capabilities of convolutional neural networks against radiomics features in computed tomography imaging. Invest Radiol. 2022;57(3):171–7.
17. Varghese BA, Fields BKK, Hwang DH, Duddalwar VA, Matcuk GR Jr, Cen SY. Spatial assessments in texture analysis: what the radiologist needs to know. Front Radiol. 2023;3:1240544.
18. Bo R, Xiong Z, Huang T, Liu L, Chen Z. Using radiomics and convolutional neural networks for the prediction of hematoma expansion after intracerebral hemorrhage. Int J Gen Med. 2023;16:3393–402.
19. Zhang L, Zhuang Q, Wu G, Yu J, Shi Z, Yuan Q, Yu J, Hu J. Combined radiomics model for prediction of hematoma progression and clinical outcome of cerebral contusions in traumatic brain injury. Neurocrit Care. 2022;36(2):441–51.
20. Zheng RZ, Zhao ZJ, Yang XT, Jiang SW, Li YD, Li WJ, Li XH, Zhou Y, Gao CJ, Ma YB, et al. Initial CT-based radiomics nomogram for predicting in-hospital mortality in patients with traumatic brain injury: a multicenter development and validation study. Neurol Sci. 2022;43(7):4363–72.
21. Swamiyappan SS, Visweswaran V, Bathala RT, Krishnaswamy V, Davuluri VS, Sridhar A, Ganesh K, Vivek V, Bathala RT. Biochemical and radiological factors for prognostication of traumatic brain injury: an institutional experience. Cureus. 2023;15(6):e40999.
22. Danilov G, Afandiev R, Pogosbekyan E, Goraynov S, Pronin I, Zakharova N. Radiomics enhances diagnostic and prognostic value of diffusion kurtosis imaging in diffuse axonal injury. Stud Health Technol Inform. 2023;309:287–91.
23. Arab A, Chinda B, Medvedev G, Siu W, Guo H, Gu T, Moreno S, Hamarneh G, Ester M, Song X. A fast and fully-automated deep-learning approach for accurate hemorrhage segmentation and volume quantification in non-contrast whole-head CT. Sci Rep. 2020;10(1):19389.
24. Schmitt N, Mokli Y, Weyland CS, Gerry S, Herweh C, Ringleb PA, Nagel S. Automated detection and segmentation of intracranial hemorrhage suspect hyperdensities in non-contrast-enhanced CT scans of acute stroke patients. Eur Radiol. 2022;32(4):2246–54.

Publisher's Note